Available online at www.sciencedirect.com
ScienceDirect
Ceramics International 35 (2009) 541–546
CERAMICS INTERNATIONAL
www.elsevier.com/locate/ceramint

# Effect of $MnO_2$ addition on microstructure and electrical properties of $ZnO–V_2O_5$-based varistor ceramics

C.-W. Nahm *

*Department of Electrical Engineering, Dongeui University, Busan 614-714, Republic of Korea*

Received 22 May 2007; received in revised form 12 November 2007; accepted 6 January 2008
Available online 6 April 2008

**Abstract**

The microstructure and electrical properties of ternary system ZnO–0.5 mol% $V_2O_5$–$MnO_2$ ceramics sintered were investigated in accordance with $MnO_2$ content by sintering at 900 °C. For all samples, the microstructure of the ternary system ZnO–$V_2O_5$–$MnO_2$ ceramics consisted of mainly ZnO grain and secondary phase $Zn_3(VO_4)_2$. The incorporation of $MnO_2$ to the binary system ZnO–$V_2O_5$ ceramics was found to restrict the abnormal grain growth of ZnO. The breakdown field in the *E–J* characteristics increased from 175 to 992 V/cm with the increase of $MnO_2$ content. The incorporation of $MnO_2$ improved non-ohmic properties by increasing non-ohmic coefficient. The highest non-ohmic coefficient (27.2) in the ternary system ZnO–0.5 mol% $V_2O_5$–$MnO_2$ was obtained for $MnO_2$ content of 2.0 mol%.
© 2008 Elsevier Ltd and Techna Group S.r.l. All rights reserved.

*Keywords:* Ternary system ZnO–$V_2O_5$–$MnO_2$; Electrical properties; Varistor ceramics

## 1. Introduction

In recent years, electronic systems have migrated towards the manufacture of increased density circuits, with the same capability obtainable in a smaller package or increased capability in the same package. This results in a greater susceptibility to various surges, such as transient over-voltage and electrostatic discharge (ESD). Once attacked by surge, electronic systems can be destroyed in very short time. Zinc oxide doped with several different metal oxides is smart semiconducting electronic ceramic device possessing the non-ohmic properties, which exhibit abruptly increasing current in accordance with increasing voltage. This non-ohmicity of voltage–current properties is due to the presence of a double Schottky barrier formed at active grain boundaries containing many trap states. Owing to highly non-ohmic properties, these ceramic devices are used widely in the field of overvoltage protection systems from electronic circuits to electric power systems [1,2]. The zinc oxide varistor ceramics cannot exhibit a non-ohmic behavior without adding the heavy elements with large ionic radii such as Bi, Pr, Ba, and so on. Commercial $Bi_2O_3$- and $Pr_6O_{11}$-based ZnO varistor ceramics cannot be co-fired with a silver inner-electrode (mp 961 °C) in multilayered chip component because of high sintering temperature above 1000 °C [3,4]. Therefore, it requires studying the new varistor ceramics in order to use a silver inner-electrode. Among various ceramics, one is the binary system ZnO–$V_2O_5$ [5–9]. These systems can be sintered at a relatively low temperature of about 900 °C. This is important for the application in which it can be a multilayer chip component, because it can be cofired with a silver inner-electrode without using the expensive palladium or platinum metals.

To develop the non-ohmic ceramics of high performance, it is very important to comprehend the effects of the additives on non-ohmic properties. It is known that the Mn additives are generally included to improve the non-ohmic properties in $Bi_2O_3$-doped ZnO varistors [10,11]. In this paper, the effect of $MnO_2$ addition on the microstructure and electrical properties of the ternary system ZnO–0.5 mol% $V_2O_5$–$MnO_2$ (ZVM) was examined. Further the feasibility of using ZVM system to fabricate multilayer chip varistors will be studied.

## 2. Experimental procedure

### 2.1. Sample preparation

Reagent-grade raw materials were prepared for ZnO varistor ceramics with ternary composition expression, such as $(99.5 - x)$ mol% ZnO + 0.5 mol% $V_2O_5$ + $x$ mol% $MnO_2$ ($x$ = 0.0, 0.25, 0.5, 1.0, 2.0). Raw materials were mixed by ball

* Tel.: +82 51 890 1669; fax: +82 51 890 1664.
*E-mail address:* cwnahm@dongeui.ac.kr.

0272-8842/$34.00 © 2008 Elsevier Ltd and Techna Group S.r.l. All rights reserved.
doi:10.1016/j.ceramint.2008.01.010

milling with zirconia balls, acetone, and polyvinyl butyl alcohol (PVB) in a polypropylene bottle for 24 h. The mixture was dried at 120 °C for 12 h and granulated by sieving 100-mesh screen to produce starting powder. The powder was uniaxially pressed into discs of 10 mm in diameter and 2 mm in thickness at a pressure of 80 MPa. The discs were sintered at 900 °C in air for 3 h. The final samples were about 8 mm in diameter and 1.0 mm in thickness. Silver paste was coated on both faces of the samples and ohmic contacts were formed by heating at 600 °C for 10 min. The electrodes were 5 mm in diameter.

### 2.2. Microstructure measurement

The microstructure was examined by a scanning electron microscope (SEM, Hitachi S2400). The average grain size ($d$) was determined by the lineal intercept method [12]. The compositional analysis of the selected areas was determined by an attached energy dispersion X-ray analysis (EDX) system. The crystalline phases were identified by powder X-ray diffraction (XRD, Model D/max 2100, Rigaku, Japan) with Cu K$\alpha$ radiation. The sintered density ($\rho$) was measured by the Archimedes method.

### 2.3. Electrical measurement

The $E$–$J$ characteristics of the samples were measured using a Keithley 237 unit. The breakdown field ($E_B$) was measured at a current density of 1.0 mA/cm$^2$ and the leakage current density ($J_L$) was measured at 0.80 $E_B$. In addition, the non-ohmic coefficient ($\alpha$) was determined from $\alpha = 1/(\log E_2 - \log E_1)$,

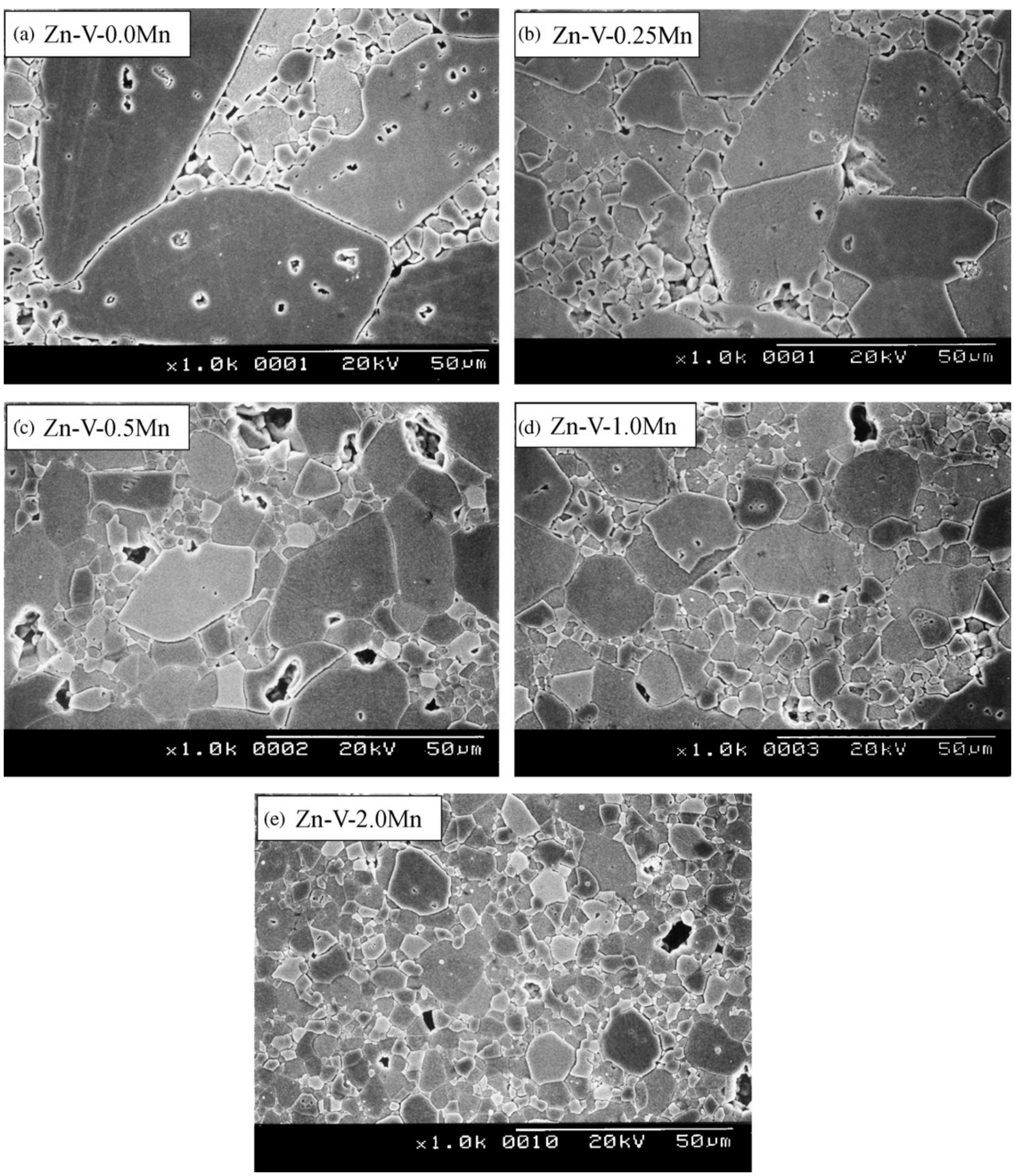


Fig. 1. SEM micrographs of the ternary system ZVM ceramics for different $MnO_2$ contents.

Table 1
Microstructure, *E–J*, and *C–V* characteristic parameters of the ternary system ZVM ceramics for different $MnO_2$ contents

| $MnO_2$ content (mol%) | $d$ (μm) | $\rho$ (g/cm$^3$) | $E_B$ (V/cm) | $v_{gb}$ (V/gb) | $\alpha$ | $J_L$ (mA/cm$^2$) | $N_d$ ($\times 10^{18}$/cm$^3$) | $\Phi_b$ (eV) | $N_t$ ($\times 10^{12}$/cm$^2$) |
|---|---|---|---|---|---|---|---|---|---|
| 0.0 | 16.1 | 5.53 | 175 | 0.28 | 2.2 | 0.82 | 0.16 | 1.10 | 1.27 |
| 0.25 | 12.2 | 5.50 | 535 | 0.65 | 11.4 | 0.88 | 0.57 | 1.95 | 3.23 |
| 0.5 | 8.4 | 5.47 | 699 | 0.58 | 16.8 | 0.66 | 0.72 | 1.47 | 3.15 |
| 1.0 | 7.9 | 5.48 | 781 | 0.62 | 24.9 | 0.45 | 0.49 | 1.68 | 2.77 |
| 2.0 | 5.2 | 5.51 | 992 | 0.52 | 27.2 | 0.17 | 0.18 | 1.99 | 1.83 |

where $E_1$ and $E_2$ are the electric fields corresponding to 1.0 and 10 mA/cm$^2$, respectively. 5 samples (sintered for the same time) were used for all electrical measurements and their average value is presented.

The capacitance–voltage (*C–V*) characteristics were measured at 1 kHz and 1 $V_{rms}$ using a RLC meter (QuadTech 7600) and an electrometer (Keithley 617). The donor density ($N_d$) of ZnO grains and the barrier height ($\Phi_b$) at the grain boundary were determined from the slope and intercept of straight line, respectively, using the equation $(1/C_b - 1/2C_{b0})^2 = 2(\Phi_b + v_{gb})/q\varepsilon \cdot N_d$ proposed by Mukae et al. [13], where $C_b$ is the capacitance per unit area of a grain boundary, $C_{b0}$ is the value of $C_b$ when $v_{gb} = 0$, $v_{gb}$ is the applied voltage per grain boundary, $q$ is the electronic charge, and $\varepsilon$ is the permittivity of ZnO ($\varepsilon = 8.5\varepsilon_0$). The density of interface states ($N_t$) at the grain boundary was determined by the equation $N_t = (2\varepsilon N_d \Phi_b/q)^{1/2}$ [13] using the value of the donor concentration and barrier height obtained above.

## 3. Results and discussion

Fig. 1 shows the SEM micrographs of the ternary system ZVM ceramics for different $MnO_2$ contents. It can be intuitively seen that the grain structure is very heterogeneously distributed throughout the samples. The binary system ZnO–$V_2O_5$ ceramics without $MnO_2$ shows very abnormal grain growth. However, the grain is uniformed in size with the increase of $MnO_2$ content. Therefore the incorporation of $MnO_2$ effectively restricted the abnormal grain growth. As the $MnO_2$ content increased, the average grain size of the ternary system ZVM ceramics decreased in order of 12.2–5.2 μm, respectively, compared to 16.1 μm for $MnO_2$-undoped sample. However, the incorporation of $MnO_2$ did not significantly modify the densification. The sintered density of the ternary system ZVM ceramics was in the range of 94.6–95.7% of theoretical density (TD) (pure ZnO, TD = 5.78 g/cm$^3$) with the increase of $MnO_2$ content.

The XRD patterns of the ternary system ZVM ceramics are shown in Fig. 2. These patterns revealed the presence of $Zn_3(VO_4)_2$ as a secondary phase, in addition to primary phase of hexagonal ZnO. The revealed phases are identical to those in the binary system ZnO–$V_2O_5$ ceramics. No secondary phase related to $MnO_2$ is detected. The EDX microanalysis for the ternary system ZnO–0.5 mol% $V_2O_5$–2.0 mol% $MnO_2$ ceramics is shown in Fig. 3. No peak for V species is found at the grain interior within EDX detection limit though the ion radius of V is smaller than that of Zn. This means the V species are not dissolved to ZnO grain. However, the Mn species was found to exist at the grain interior, in addition to Zn. On the other hand, it is found that the grain boundaries contain V and Mn species. As a result, the Mn species exist not only at grain boundaries but also grain interiors. The more detailed microstructural parameters are summarized in Table 1.

Fig. 4 shows the electric field–current density (*E–J*) characteristics of the ternary system ZVM ceramics for

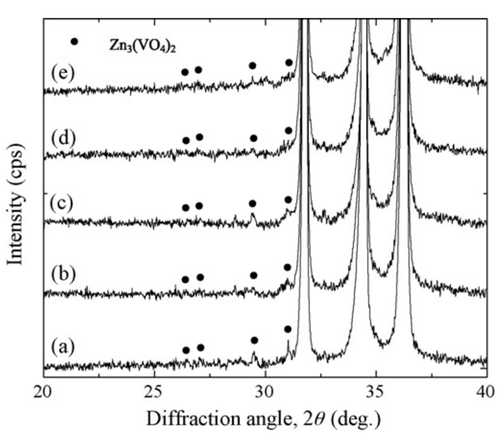


Fig. 2. XRD patterns of the ternary system ZVM ceramics for different $MnO_2$ contents: (a) 0.0 mol%, (b) 0.25 mol%, (c) 0.5 mol%, (d) 1.0 mol%, and (e) 2.0 mol%.

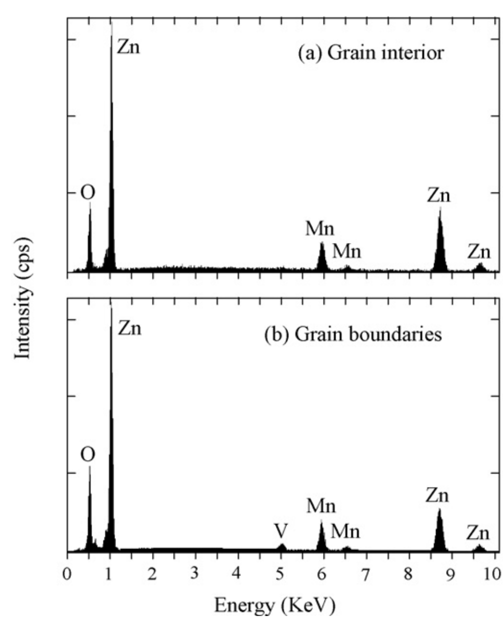


Fig. 3. EDX microanalysis of the ternary system ZnO–0.5 mol% $V_2O_5$–2.0 mol% $MnO_2$ ceramics.

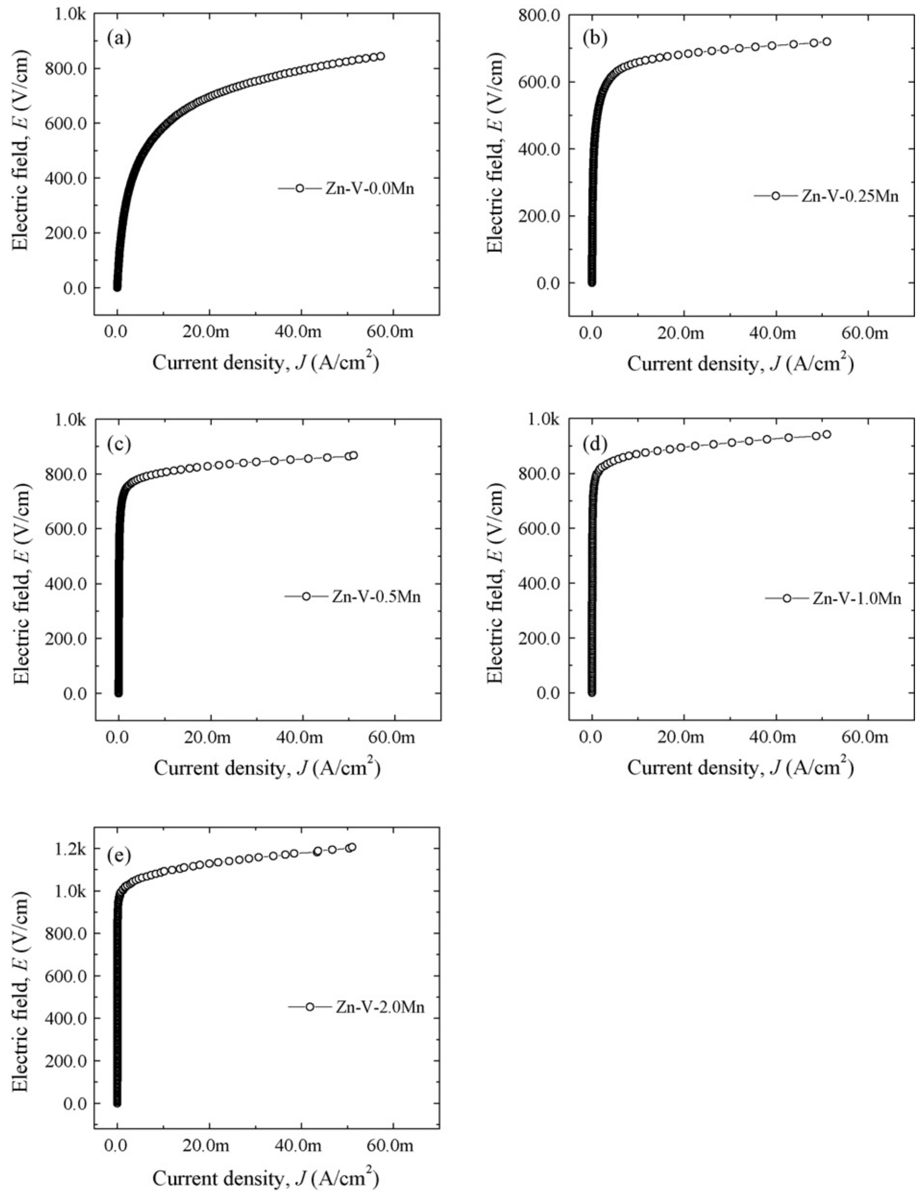


Fig. 4. *E–J* characteristics of the ternary system ZVM ceramics for different $MnO_2$ contents.

different $MnO_2$ contents. The non-ohmic properties are characterized by non-ohmicity in the *E–J* characteristic curve. The curves show that the conduction characteristics divide into two regions: ohmic region before breakdown field and non-ohmic region after breakdown field. The sharper the knee of the curves between the two regions, the better the non-ohmic properties. The $MnO_2$-undoped samples showed very poor non-ohmic properties. On adding more $MnO_2$, the knee gradually becomes more pronounced and the non-ohmic properties are enhanced. Therefore, the incorporation of $MnO_2$ seems to remarkably enhance non-ohmic properties. The breakdown field ($E_B$) greatly increased from 175 to 992 V/cm with the increase of $MnO_2$ content. The increase of $E_B$ with the increase of $MnO_2$ content can be explained by the increase in the grain boundary density owing to the decrease in the average ZnO grain size, as shown in Fig. 5. The breakdown voltage per grain boundary ($\upsilon_b$) is calculated by the following equation: $V_B = N_b \cdot \upsilon_b = (D/d)\upsilon_b$, where $V_B$ is breakdown voltage, $N_b$ is the number of grain boundaries, $d$ is the average grain size, and $D$ is the thickness of sample. The $\upsilon_b$ was in the range of 0.5–0.6 V with the increase of $MnO_2$ content.

Fig. 6 shows the variation of the non-ohmic coefficient ($\alpha$) and the leakage current density ($J_L$) of the ternary system ZVM ceramics as a function of $MnO_2$ content. The $\alpha$ and $J_L$ value for samples are derived from the *E–J* curves shown in Fig. 4. The calculated $\alpha$ value of $MnO_2$-undoped samples was only 2.2, whereas the $\alpha$ value of $MnO_2$-doped samples greatly increased from 11.4 to 27.2. In particular, when the $MnO_2$ content is more than 1.0 mol%, the samples exhibited relatively good varistor properties. The maximum of non-ohmic coefficient was 27.2, obtained from the addition of 2.0 mol% $MnO_2$. It should be noticed that the non-ohmic coefficient above 27 in the ternary system ZVM ceramics is much higher than the non-ohmic coefficient (13–18) for

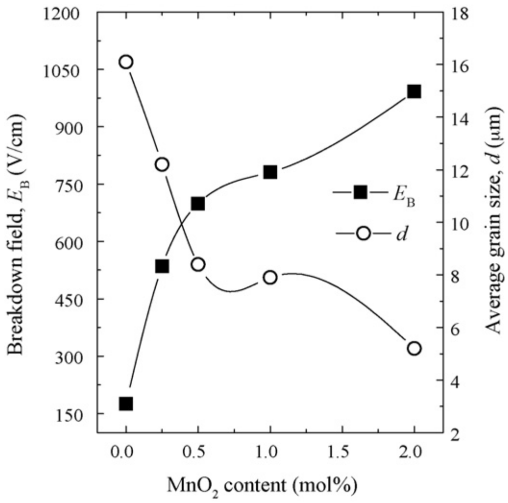


Fig. 5. Breakdown voltage and average grain size of the ternary system ZVM ceramics as a function of $MnO_2$ content.

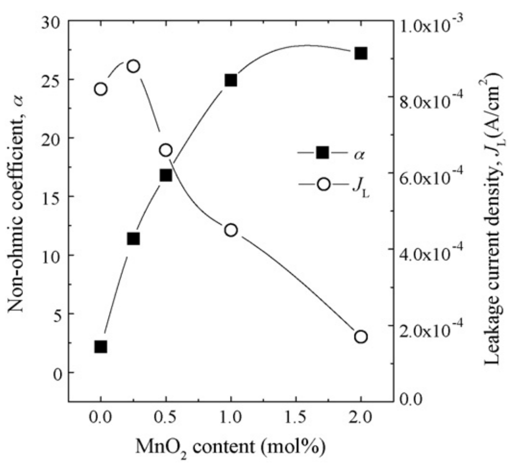


Fig. 6. Non-ohmic coefficient and leakage current density of the ternary system ZVM ceramics as a function of $MnO_2$ content.

ternary system $ZnO–Bi_2O_3–CoO$ (or MnO) ceramics [14]. As a result, the ternary system ZVM ceramics doped with $MnO_2$ content of 2.0 mol% could be applied to low voltage varistors because of low breakdown voltage per grain boundary and high non-ohmic coefficient. On the other hand, when the $MnO_2$ content is small below 0.25 mol%, the $J_L$ value increased. The further addition of $MnO_2$ caused the $J_L$ value to decrease. 2.0 mol% $MnO_2$-doped samples significantly decreased up to 0.17 mA/cm$^2$. The more detailed $E–J$ characteristic parameters are summarized in Table 1.

Fig. 7 shows the capacitance–voltage ($C–V$) characteristics of the ternary system ZVM ceramics for different $MnO_2$ contents. The $C–V$ parameters such as the donor density ($N_d$), barrier height ($\Phi_b$), and density of interface states ($N_t$) are basically derived from Fig. 7 and are summarized in Table 1. The $N_d$ value was in the range of $0.16 \times 10^{18}$–$0.72 \times 10^{18}$/cm$^3$ and changed with a peak value of $0.72 \times 10^{18}$/cm$^3$ at 0.5 mol% $MnO_2$. The $MnO_2$ is like to act as a donor due to the increase of donor density in the range of $MnO_2$ addition, compared with

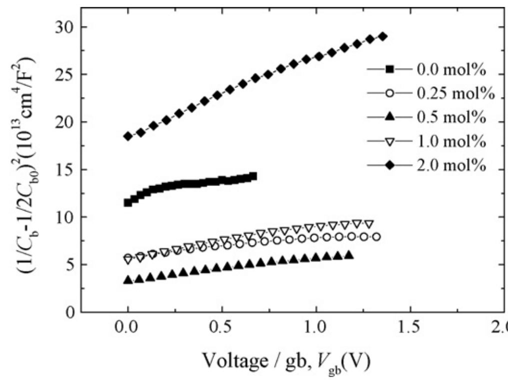


Fig. 7. $C–V$ characteristics of the ternary system ZVM ceramics for different $MnO_2$ contents.

$MnO_2$-undoped sample. The $\Phi_b$ value, on the whole, increased in the range of 1.10–1.99 eV with the increase of $MnO_2$ content. This coincides with the variation of $\alpha$ in $E–J$ characteristics. That is, the higher $\Phi_b$ gives rise to the higher $\alpha$ in terms of the conduction mechanism. On the other hand, the $N_t$ value of $MnO_2$-doped samples is higher than that of $MnO_2$-undoped sample, and when $MnO_2$ content is small less than 0.25 mol%, the $N_t$ value increased, whereas further addition decreased the $N_t$ value. The $N_t$ is directly connected with the $N_d$ and $\Phi_b$. In other words, the $N_t$ is estimated by the variation rate in the $N_d$ and $\Phi_b$. According to this reason, it can be understood that the $N_t$ is changed with the increase of $MnO_2$ content.

As a result, it can be seen that the incorporation of $MnO_2$ to the binary system $ZnO–V_2O_5$ ceramics remarkably improves the non-ohmic properties, namely, it makes the non-ohmic coefficient higher and the leakage current density smaller.

## 4. Conclusions

The effect of $MnO_2$ addition on the microstructure and electrical properties of the binary system $ZnO–V_2O_5$ ceramics were investigated. For all samples, the microstructure of the ternary system $ZnO–V_2O_5–MnO_2$ ceramics consisted of mainly ZnO grain and $Zn_3(VO_4)_2$ as a secondary phase. The addition of $MnO_2$ to the binary system $ZnO–V_2O_5$ ceramics was found to restrict the abnormal grain growth of ZnO. The highest non-ohmic properties in the ternary system ZnO–0.5 mol% $V_2O_5$–$MnO_2$ ceramics were obtained for $MnO_2$ content of 2.0 mol%, with the non-ohmic coefficient of 27.2. The $MnO_2$ acted as a donor due to the increase of donor density, compared with $MnO_2$-unoped sample. Conclusively, it is assumed that the ternary system ZVM ceramics are suitable materials to fabricate multilayer chip varistors, because it can be cofired with a silver inner-electrode.

## References


[1] L.M. Levinson, H.R. Philipp, Zinc oxide varistor—a review, Am. Ceram. Soc. Bull. 65 (1986) 639–646.

[2] T.K. Gupta, Application of zinc oxide varistor, J. Am. Ceram. Soc. 73 (1990) 1817–1840.

[3] C.-W. Nahm, The nonlinear properties and stability of $ZnO-Pr_6O_{11}-CoO-Cr_2O_3-Er_2O_3$ ceramic varistors, Mater. Lett. 47 (2001) 182–187.

[4] C.-W. Nahm, ZnO-$Pr_6O_{11}$-CoO-$Cr_2O_3$-$Er_2O_3$-based ceramic varistors with high stability of nonlinear properties, J. Mater. Sci. Lett. 21 (2002) 201–204.
[5] J.-K. Tsai, T.-B. Wu, Non-ohmic characteristics of ZnO-$V_2O_5$ ceramics, J. Appl. Phys. 76 (1994) 4817–4822.
[6] J.-K. Tsai, T.-B. Wu, Microstructure and nonohmic properties of binary ZnO-$V_2O_5$ ceramics sintered at 900 °C, Mater. Lett. 26 (1996) 199–203.
[7] C.T. Kuo, C.S. Chen, I.-N. Lin, Microstructure and nonlinear properties of microwave-sintered ZnO-$V_2O_5$ varistors: I, effect of $V_2O_5$ doping, J. Am. Ceram. Soc. 81 (1998) 2942–2948.
[8] H.-H. Hng, K.M. Knowles, Characterisation of $Zn_3(VO_4)_2$ phases in $V_2O_5$-doped ZnO varistors, J. Eur. Ceram. Soc. 19 (1999) 721–726.
[9] H.-H. Hng, L. Halim, Grain growth in sintered ZnO-1 mol% $V_2O_5$ ceramics, Mater. Lett. 57 (2003) 1411–1416.
[10] G.S. Pike, S.R. Kurtz, P.L. Gourley, H.R. Philipp, L.M. Levinson, Electroluminescence in ZnO-varistors, J. Appl. Phys. 57 (1985) 5512–5518.
[11] L.M. Levinson, Advances in varistor technology, American Ceramic Society, Westerville Ohio, 1989, pp. 31–53.
[12] J.C. Wurst, J.A. Nelson, Lineal intercept technique for measuring grain size in two-phase polycrystalline ceramics, J. Am. Ceram. Soc. 55 (1972) 109–111.
[13] M. Mukae, K. Tsuda, I. Nagasawa, Capacitance-vs.-voltage characteristics of ZnO varistor, J. Appl. Phys. 50 (1979) 4475–4476.
[14] M. Matsuoka, Nonlinear properties of zinc oxide ceramics, Jpn. J. Appl. Phys. 10 (1971) 736.